NJC

Accepted Manuscript

This is an *Accepted Manuscript*, which has been through the Royal Society of Chemistry peer review process and has been accepted for publication.

Accepted Manuscripts are published online shortly after acceptance, before technical editing, formatting and proof reading. Using this free service, authors can make their results available to the community, in citable form, before we publish the edited article. We will replace this *Accepted Manuscript* with the edited and formatted *Advance Article* as soon as it is available.

You can find more information about *Accepted Manuscripts* in the Information for Authors.

Please note that technical editing may introduce minor changes to the text and/or graphics, which may alter content. The journal's standard Terms & Conditions and the Ethical guidelines still apply. In no event shall the Royal Society of Chemistry be held responsible for any errors or omissions in this *Accepted Manuscript* or any consequences arising from the use of any information it contains.

ROYAL SOCIETY OF CHEMISTRY

www.rsc.org/njc

Color graphic:

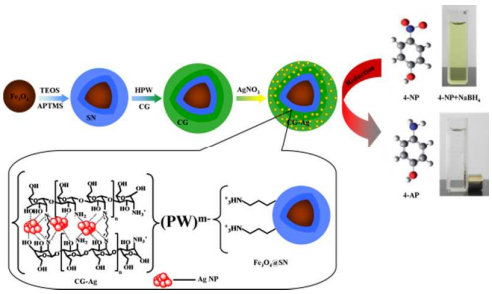

Magnetic chitosan-based core-shell composites have been prepared employing phosphotungstic acid as layer-linker and chitosan as green reducing agent.

NJC

RSCPublishing

PAPER

In situ preparation of uniform Ag NPs onto multifunctional Fe_3O_4@SN/HPW@CG towards efficient reduction of 4-nitrophenol

Cite this: New J. Chem. , 2014, 00, 0000

Received 00th January 2014,
Accepted 00th January 2014

DOI: 10.1039/x0xx00000x

www.rsc.org/njc

Zhenzhen Wang, Shangru Zhai,* Bin Zhai, Zuoyi Xiao, Feng Zhang, and Qingda An*[a]

Novel protocol towards multifunctional magnetic organic-inorganic core-shell nanostructured catalysts of Fe_3O_4@SN/HPW@CG-Ag with tailored properties was presented in this work. Such designed nanocomposites congregated the properties and functions of single component into a whole. For instance, Fe_3O_4 cores protected by amino-functionalized SiO_2 shell endowed the composites with superparamagnetism (28.6 emu g^{-1}) and thereby facilitated the process of separation and recovery. Phosphotungstic acid, as a bridging agent, provided strong interaction for the anchoring of glutaraldehyde cross-linked chitosan onto the surface of Fe_3O_4@SN. More interestingly, chitosan could simultaneously behave as stabilizer and reductant for the in situ synthesis of "green" Ag NPs without addition any other reducing agent or organic solvent, and Ag NPs furnished the compounds with catalytic performance. Further the size, loading of Ag NPs and the thickness of chitosan layer were all controllable. Meaningfully, the as-synthesized catalyst Fe_3O_4@SN/HPW@CG-Ag exhibited exceptional catalytic performance for the reduction of 4-nitrophenol in the presence of sodium borohydride (the reaction was accomplished within 7 min) and could be reused at least 10 times with good stability by means of convenient magnetic separation. Thence, the design philosophy of the multifunctional robust Ag-based nanocatalysts may offer a reference for the synthesis of other catalyst systems with long-term stability.

Introduction

For the past few years, multifunctional organic-inorganic core-shell nanostructured composites are burgeoning as an interesting family, which have received comprehensive attention for their applications in various realms such as biomedicine[1,2] and catalysis,[3-6] because they could integrate diversiform functions and features of the individual component within a single part. That is such nanocomposites not only have flexibility and varieties of functional groups from polymers, also have thermal stability along with mechanical strength of inorganic components.[7,8] Especially, hierarchical organic-inorganic core-shell nanocatalysts have received widespread attraction for their outstanding properties. Over the years, nanosized noble-metal particles have attracted extraordinary interest for their unexpectedly highly catalytic properties toward varieties of reactions,[9-13] due to their extremely high surface area-to-volume ratio. Amongst them, Ag NPs have been one of the most interesting topics in consideration of its relatively cheap price. Whereas, there are several drawbacks that greatly prohibit it from large-scale use.[14] To begin with, the neat Ag NPs are apt to aggregation due to their higher surface energy, resulting in a significant reduction of their catalytic activity; on the side, the separation of smaller Ag NPs from the catalytic system is tough and could not be reused afterwards. Moreover, the preparation procedure of Ag NPs always involved in various reagents such as sodium borohydride, hydrazine hydrate, which are hazardous, toxic to both environment and organism. As remarked above, it still remains a bottleneck problem to design and synthesis "green" NPs[15,16] with long-term stability and reusability.

In the first place, to overcome the separation and recovering problems, magnetic nanoparticles are generally used for inorganic supports in the synthesis of organic-inorganic composite materials in view of their distinct physical properties and superparamagnetic nature. Speaking of which, Fe_3O_4 NPs have attracted much attention because they could be expediently separated from reaction system by applying an external magnetic field and recovered for iterative use.[17-22] Hence, it is possible to control reactions on or off and accordingly reduce the operational costs. However, Fe_3O_4 NPs are liable to conglobation, thus the surface modification or coating seems to be of prime importance. As is known to all, silica is one of the most ideal materials to inhibit Fe_3O_4 NPs from damage and aggregation and endows the magnetic nanoparticles with functionality. Hereafter, silica shell could be functionalized by 3-aminopropyltrimethoxysilane (APTMS) through the saline coupling reaction[23] for further application (denoted as Fe_3O_4@SN).

During the past decade, to prevent Ag NPs from aggregation, the most effective approach is to immobilize them on various supports such as activated carbon, silica,

dendrimers, and polymers. Taking into consideration of the development of cost-efficient and environmentally benign heterogeneous catalysts, it remains a great challenge to select a suitable material to green synthesize and efficiently stabilize Ag NPs.[24-27] Noteworthily, chitosan (CS), a naturally occurring, biodegradable, biocompatible, and non-toxic polysaccharide, contains abundant hydroxyl, amino active functional groups, what make it an efficient adsorbent and stabilizer as well as reductant for metal ions and metal nanoparticals and is receiving increasing attention as matrix materials.[28-35] Thence, we choose CS as the in situ green reductant and stabilizer of Ag NPs in aqueous solution without addition any other reducing agent or organic solvent. Furthermore, in order to increase the amount of Ag^+ absorbed, the stabilization and mechanical strength of CS layer,[36] we prefer glutaraldehyde (GLA), a more effective cross-linking agent than other aldehydes,[37] as cross-linker to release more free amino and hydroxyl active groups to bind with more Ag^+. Even though there are several reports on the adsorption of metal ions with GLA cross-linked CS (CG),[38-40] but to the best of our knowledge, this is the first time to use CG to adsorb and in situ reduce Ag^+ in aqueous solution and the impact of different volume of GLA solution was further investigated hereinbelow. As discussed above, the problems of separation, recovering, aggregation and reduction of Ag NPs are all overcome.

Nonetheless, how to effectively integrate CG onto the surface of Fe_3O_4@SN to form an intact whole is a big deal because they are both positively charged. Herein, phosphotungstic acid (HPW), a typical polyanion, was chosen as a bridging agent for the immobilization process and provided strong electrostatic interactions between CG and Fe_3O_4@SN. As far as we know, this is the first time to use the support containing HPW to immobilize Ag NPs. In addition, the influence of addition amount of HPW is also discussed below. Up to this point, the multifunctional magnetic organic-inorganic hierarchical core-shell nanostructured catalysts are finally achieved (Scheme 1).

The as-prepared Fe_3O_4@SN/HPW@CG-Ag catalysts successfully realize the combination of functions and features from single component. For example, Fe_3O_4 core predigests the separation and recovery process, thereby saving energy and more environmentally benign. CG provides a method for the preparation of "green" NPs without introducing any other reducing agent or organic solvent. The structure and composition of the composite nanocatalysts were thoroughly characterized by Scanning Electron Microscope (SEM), Transmission Electron Microscope (TEM), X-ray Diffraction (XRD), Energy Dispersive X-ray Analysis (EDX), Fourier Transform Infrared Spectroscopy (FTIR), X-Ray Photoelectron Spectroscopy (XPS) and Vibrating Sample Magnetometer (VSM). Furthermore, as a robust magnetically recoverable nanocatalyst, its catalytic performance, reusability along with the corresponding kinetic were also investigated applying the reduction of 4-nitrophenol (4-NP) in the presence of $NaBH_4$. Considering that 4-NP is one of the most common organic contaminants in wastewaters and has been listed as "priority pollutant" by US Environmental Protection Agency (EPA) as a result of its high solubility and stability in water. On the other hand, its daughter derivatives 4-aminophenol (4-AP) is a vital intermediate for the preparation of many analgesic/antipyretic drugs and at the same time is also highly important in photographic development, corrosion inhibition and dyeing agent and so on.

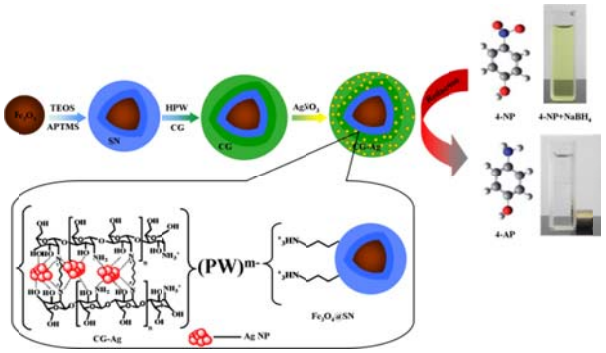

Scheme 1 Preparation process of multifunctional Fe_3O_4@SN/HPW@CG-Ag composites with tailored properties.

Experimental section

Chemicals

Ferric chloride hexahydrate ($FeCl_3 \cdot 6H_2O$), tetraethoxysilane (TEOS), ethanol (EtOH), ethylene glycol (EG), methanol (CH_3OH) and glacial acetic acid (CH_3COOH) were purchased from Tianjin Kermel Chemical Reagent Factory, China. Trisodium citrate dihydrate (Na_3Cit), phosphotungstic acid hydrate (HPW), and chitosan (CS) were purchased from Sinopharm Chemical Reagent Co., Ltd., China. Sodium acetate anhydrous (NaOAc) and ammonia water ($NH_3 \cdot H_2O$, 25~28 wt%) were supplied by Shenyang Chemical Plant, China. 3-Aminopropyl trimethoxysilane (APTMS), glutaraldehyde (GLA, 50%), 4-nitrophenol (4-NP), and sodium borohydride ($NaBH_4$) were purchased from Aladdin Chemistry Co., Ltd., China. Silver nitrate ($AgNO_3$) was obtained from Tianjin chemical corporation, China. All chemicals were analytical grade and used as received without any further purification.

Synthesis of Fe_3O_4@SN/HPW@CG

Based on the work of our group.[41,42] The magnetic Fe_3O_4 NPs were firstly synthesized through a solvothermal method. Briefly, $FeCl_3 \cdot 6H_2O$ (1.62 g), NaOAc (4.0 g) and Na_3Cit (1.5 g) were dissolved in EG (60 mL) with magnetic stirring at room temperature for 1 h. The obtained homogeneous yellow solution was then transferred into a Teflon-lined stainless-steel autoclave (100 mL) and sealed to heat at 200 °C for 12 h. Thereafter, the autoclave was naturally cooled to room temperature. The obtained black Fe_3O_4 NPs were collected with a magnet and washed, finally re-dispersed in deionized water (80 mL) to form magnetofluid. Later on, the magnetofluid (20 mL) was mixed with ethanol (150 mL) under continuous mechanical stirring for 15 min at 30 °C in advance of the addition of $NH_3 \cdot H_2O$ (0.6 mL). After being continuous stirring for 30 min, TEOS (1.0 mL) was added drop wise slowly. The mixture was stirred for another 35 min before the addition of APTMS (0.07 ml). After stirring for 4 h, the resulting Fe_3O_4@SN was collected and washed. Whereafter the dried Fe_3O_4@SN (1.5 g) was added to methanol solution (30 mL) of HPW (0.1, 0.25, 0.35 and 0.5 g HPW) under mechanical stirring at 50 °C for 3 h. Then the resulting Fe_3O_4@SN/HPW was dried. The impact of HPW amount on the thickness of CG layer was investigated in this step. The as-prepared Fe_3O_4@SN/HPW NPs above were dispersed into deionized water (20 mL) with constant stirring at 50 °C. Then under continuous mechanical stirring, acetic acid solution (20 mL) of

CS (1.0 g CS in 100 mL 2% HOAc) was added to the mixture, GLA aqueous solution (10, 20, 30 mL, 5 wt%) was added drop wise subsequently and the reaction was continued for another 1.5 h. Afterwards, the resultant products were rinsed and dried for further application.

Preparation of multifunctional Fe_3O_4@SN/HPW@CG-Ag

To prepare Fe_3O_4@SN/HPW@CG-Ag, in a typical procedure, Fe_3O_4@SN/HPW@CG (0.5 g) was dispersed into $AgNO_3$ aqueous solution (60 mL). After continuing stirring at 80 ^oC for 4 h, the reaction product was cooled naturally to room temperature and separated with a magnet. The precipitate was then washed with deionized water to remove those free Ag NPs that were not embedded into the CG layer. Finally, the as-prepared Fe_3O_4@SN/HPW@CG-Ag was dried. Furthermore, the relationship between the size and quantity of Ag NPs stabilized by CG layer and the feeding concentration of $AgNO_3$ was studied. When the concentration of $AgNO_3$ was $X \times 10^{-3}$ M, the as-prepared catalyst was denoted as Fe_3O_4@SN/HPW@CG-Ag_X. The Fe_3O_4@SN/HPW@CG-Ag in the article refers to Fe_3O_4@SN/HPW@CG-Ag_{10}, unless otherwise noted.

Catalytic reduction of 4-NP in aqueous medium

For purpose of assessing the catalytic properties of the as-prepared multifunctional catalyst Fe_3O_4@SN/HPW@CG-Ag, the reduction of 4-NP with $NaBH_4$ at room temperature in aqueous solution was conducted as a model reaction. Typically, 4-NP aqueous solution (0.7 mL, 5 mM), deionized water (17 mL), and freshly prepared $NaBH_4$ aqueous solution (1.3 mL, 0.2 M) were mixed in three-necked flask under nitrogen atmosphere, followed by the addition of Fe_3O_4@SN/HPW@CG-Ag aqueous solution (1.0 mL, 1 mg mL^{-1}). As the catalytic reaction proceeded, the bright yellow color of the solution faded gradually and the catalytic activity was monitored by a UV-vis spectrophotometer at a time interval of 1 min.

The reusability of the catalyst Fe_3O_4@SN/HPW@CG-Ag was also studied. After the reduction of 4-NP was completed, the catalysts were separated from the mixture with a magnet and washed with deionized water, then reused in the next cycle. This procedure was repeated for 11 times.

Characterization

The morphology of the as-prepared multifunctional nanoparticles was observed by JSM-6460LV scanning electron microscopy (SEM, JEOL, Japan) and JEM-2000EX transmission electron microcopy (TEM, JEOL, Japan). The elemental composition of Fe_3O_4@SN/HPW@CG-Ag composites was analyzed by X-MaxN energy dispersive X-ray analyzer (EDX, OXFORD, UK). X-ray diffraction (XRD) patterns were conducted by Shimadzu XRD-6100 diffractometer using CuKα radiation (λ = 1.54060 Å) for a 2θ range of 10^o to 80^o at the scanning speed of 8^o min^{-1}. Fourier transform infrared (FTIR) spectra were recorded on One-B FTIR spectrometer over KBr pressed pellets. The magnetization curve of the catalyst was measured through Lake Shore 7410 vibrating sample magnetometer (VSM) at room temperature. X-Ray photoelectron spectroscopy (XPS) measurements were performed by applying Thermo Scientific ESCALAB250 spectrometer (Thermo VG, USA) with monochromatic AlKa radiation (1486.6 eV). UV-vis absorption spectra were recorded by a MAPADA UV-1600PC spectrometer.

Results and discussion

The morphology and structure of the as-prepared samples at different stages were characterized by SEM and TEM. Firstly, the magnetic Fe_3O_4 NPs were synthesized by solvothermal method via high temperature reduction of Fe^{3+} salts with ethylene glycol.[43] As revealed in Fig. 1A, the Fe_3O_4 NPs are evidently spherical, uniform (~ 200 nm) and monodisperse. Then, amino-functionalized SiO_2 (SN) was coated on the surface of Fe_3O_4 through one-pot sol-gel method to form Fe_3O_4@SN core-shell structured composites. From Fig. 1B, Fe_3O_4@SN composite kept up the morphological properties of pure Fe_3O_4 and at the same time a slightly larger in size about 240 nm was observed, thus the thickness of SN is approximately 20 nm.

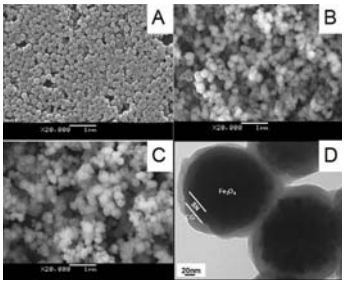

Fig. 1 SEM images of (A) Fe_3O_4, (B) Fe_3O_4@SN, (C) Fe_3O_4@SN/HPW@CG and (D) TEM image of Fe_3O_4@SN/HPW@CG.

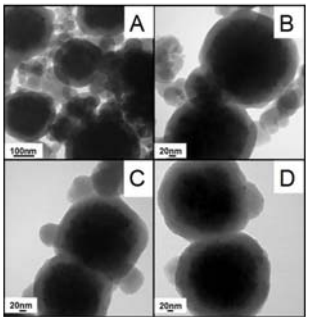

Fig. 2 TEM images of Fe_3O_4@SN/HPW@CG obtained with different HPW amounts: (A) 0 g, (B) 0.1 g, (C) 0.25 g and (D) 0.35 g.

To effectively introduce and three-dimensionally stabilize CG, we choose HPW to play the role of a bridging layer to strengthen the interaction between Fe_3O_4@SN cores and polymeric CS macromolecules, taking into account that CS layers would be swelled and accordingly leached away from preformed Fe_3O_4@SN. Meanwhile, because the surface of both Fe_3O_4@SN and CG are all positively charged under mild acidic conditions, it is difficult for the direct integration of CG onto the surface of Fe_3O_4@SN due to the electrostatic repulsion. As shown in Fig. 2A, CG is prone to self polymerization instead of coating/deposition on the surface of Fe_3O_4@SN in the absence of HPW. Conversely, the addition of HPW, as a typical polyanion, is found to be an effective method to reverse the surface positive charge of Fe_3O_4@SN to negative charge; whereby, the electrostatic attachment for negatively charged Fe_3O_4@SN/HPW with positively charged CG is favorable.

Noting that, as far as we know, this is the first time to utilize the support containing HPW to immobilize CS macromolecules and subsequently Ag NPs. The effect of HPW amount on Fe_3O_4@SN/PTA@CG is also studied by a set of experiments while keeping the other parameter unchanged. Fig. 2B-D and Fig. 1D shows the TEM images of the resultant Fe_3O_4@SN/HPW@CG composites by changing HPW amount from 0.1 g, 0.25 g, 0.35 g to 0.5 g, respectively. As illustrated in TEM images, with increasing of HPW amount, the phenomenon of CG self polymerization gradually disappear and the thickness of the outer CG shell increase visually, which show a positive correlation relationship between the shell thickness and the amount of HPW. Considering that thicker CS layers might be favorable for in-situ stabilization of uniform Ag NPs, the HPW amount used in the following experiments was fixed to 0.5 g. The introduction of CG is observed from Fig. 1C that the resultants remain spherical in shape and the size is further increased in contrast with Fe_3O_4@SN. Meanwhile, no obvious aggregation could be observed, which is crucial for the deposition of Ag. On the other hand, it could also be evident from TEM micrograph (Fig. 1D) that Fe_3O_4@SN/HPW@CG composites possess a well-defined core-shell structure with distinguishable three-layer structure including a Fe_3O_4 core (dark colored), a SN interlayer (gray colored), and a CG outerlayer (light colored) due to the distinct density.

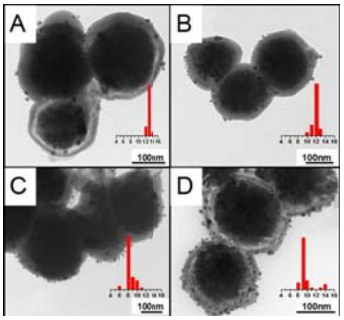

Fig. 3 TEM images of Fe_3O_4@SN/HPW@CG-Ag obtained with different $AgNO_3$ concentrations (volume of GLA is fixed to 20 mL): (A) 5×10^{-3} M (Fe_3O_4@SN/HPW@CG-Ag_5), (B) 8×10^{-3} M (Fe_3O_4@SN/HPW@CG-Ag_8), (C) 10×10^{-3} M (Fe_3O_4@SN/HPW@CG-Ag), and (D) 12×10^{-3} M (Fe_3O_4@SN/HPW@CG-Ag_{12}).

As is known to all, CS is capable to absorb, stabilize and reduce metal ions. In this study, we attempt to use the sturdy multifunctional core-shell material of Fe_3O_4@SN/HPW@CG to absorb, stabilize and in situ green reduce Ag^+. From Fig. 3, Ag NPs are formed apparently and the size and loading of Ag NPs have a lot to do with the concentration of $AgNO_3$. From the micrographs in Fig. 3, it was observed apparently that the amount of Ag NPs increased and the size of Ag NPs increased first and then decreased as $AgNO_3$ concentration is increased. In detail, when the concentration of $AgNO_3$ is 5×10^{-3} M , 8×10^{-3} M, few and large-size Ag NPs are appeared on the surface of Fe_3O_4@SN/HPW@CG (Fig. 3A, B). When the concentration increased to 10×10^{-3} M, we could appreciate that Ag NPs are mainly small-size (~ 8 nm), monodispersed and distributed in the inner and outer surfaces of CG shell (Fig. 3C). However, while the concentration further increases to 12×10^{-3} M, bigger Ag NPs are observed and the proportion of small Ag NPs decreases because of the apparent agglomeration (Fig. 3D). This trend was also observed in the literature of Zeng et al.[44]

The composite catalyst Fe_3O_4@SN/HPW@CG-Ag discussed below refers to the catalyst prepared at the concentration of 10×10^{-3} M, unless otherwise noted. The deposition of Ag on the Fe_3O_4@SN/HPW@CG NPs could also be confirmed by energy dispersive X-ray (EDX) spectroscopy. As shown in Fig. 4, the analysis of EDX spectrum proves the existence of C, N, O, Fe, Si, P, W, and Ag elements. Furthermore, a more detailed elemental Ag distribution of Fe_3O_4@SN/HPW@CG-Ag NPs is gained from the EDX mapping (Fig. 4, inset), clearly showing that Ag is evenly distributed in the composite. In addition, the mass fractions of Ag with different $AgNO_3$ concentrations (V_{GLA} = 20 mL) and GLA volumes ($C_{AgNO_3} = 10 \times 10^{-3}$ M) are summarized in Table 1.

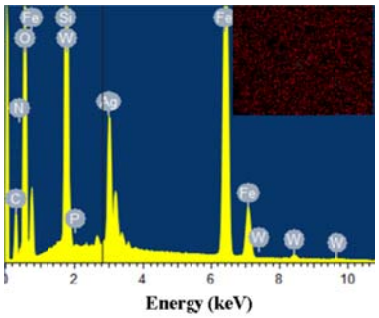

Fig. 4 EDX and elemental Ag EDX mapping (inset) of Fe_3O_4@SN/HPW@CG-Ag nanocomposite.

Table 1 The loading of Ag in Fe_3O_4@SN/HPW@CG-Ag obtained with different $AgNO_3$ concentrations and GLA volumes.

Entry	C_{AgNO_3}[a] (1×10^{-3} M)				V_{GLA}[b] (mL)		
	5	8	10	12	10	20	30
wt%(Ag)	5.52	6.98	7.92	8.48	5.96	7.92	7.46

[a] V_{GLA} = 20 mL. [b] $C_{AgNO_3} = 10\times10^{-3}$ M.

The crystallographic structure of the supports at different preparation stages and thus resultant catalysts were attested by the typical wide-angle XRD patterns (Fig. 5). The characteristic peaks at $2\theta = 30.31^o$, 35.59^o, 43.27^o, 53.61^o, 57.09^o, and 62.61^o, corresponding to (112), (211), (220), (024), (303), and (224) planes of the orthorhombic phase of Fe_3O_4,[45] are observed in all samples, revealing that the crystalline structure of the Fe_3O_4 particles was well maintained after a series of functionalizations. For Fig. 5(b), (c), (d), and (e), the apparent broad peak at around $2\theta = 23^o$ corresponded to the amorphous peak of SiO_2, indicates SiO_2 have been successfully coated on the surface of Fe_3O_4 NPs. As shown in Figure. 5(c), the XRD pattern of Fe_3O_4@SN/HPW, some additional peaks appeared, which are assigned to the Keggin structure of HPW, indicating the surely introduction of HPW as expected. After coated with CG, the diffraction peaks of HPW no longer appeared (Figure. 5(d)), which further confirm the covering of CG onto the surface of Fe_3O_4@SN/HPW. In the case of Fe_3O_4@SN/HPW@CG-Ag catalysts (Figure. 5(e)), with the exception of the characteristic peaks of Fe_3O_4, four new peaks at 2θ values of 38.1^o, 44.3^o, 64.5^o and 77.5^o (labeled with the symbol ●), corresponding to the (111), (200), (220), and (311) planes of the face centered cubic (fcc) of Ag,[46] are clearly observed, which not only prove the formation of Ag NPs but also the narrow peaks imply that Ag NPs have good crystal

structure. The facts aforementioned also confirm the formation of multifunctional hierarchical nanocatalysts.

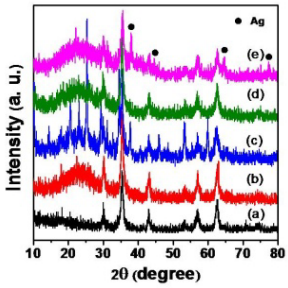

Fig. 5 Wide-angle XRD patterns of as-prepared Fe_3O_4 (a), Fe_3O_4@SN (b), Fe_3O_4@SN/HPW (c), Fe_3O_4@SN/HPW@CG (d) and Fe_3O_4@SN/HPW@CG-Ag (e), respectively.

Fig. 6 shows the FT-IR spectra of sample prepared at various stages. For all the samples studied, the peak at 567 cm^{-1} is assigned to the Fe–O stretching vibration of Fe_3O_4,[14] confirming the existence of Fe_3O_4 in all the materials. Those prominent peaks at 1081 cm^{-1}, 808 cm^{-1}, 955 cm^{-1}, and 461 cm^{-1} are corresponded to the asymmetric stretching vibration of Si−O−Si, symmetric stretching vibration of Si−O−Si, the stretching modes of surface Si–OH and the bending vibration of O–Si–O, respectively.[47,48] In addition, the typical peaks at 2940 cm^{-1} is attributed to the $–CH_2–$ stretching vibrations from APTMS component and the enhanced wide band at around 3400 cm^{-1} is attributed to the vibration of overlapping –OH and $–NH_2$ groups. These results suggest that the Fe_3O_4 NPs were successfully coated with SN layer. In Fig. 6(b), the detection of weak fingerprint bands of the Keggin structure in 800–1100 cm^{-1} region also indicate the introduction of HPW onto the surface of Fe_3O_4@SN. After the incorporation of CG on the surface of Fe_3O_4@SN/HPW (Fig. 6(c)), new peaks appeared at 1550 cm^{-1} and 1415 cm^{-1} belong to bending vibrations of $–NH_2$ and secondary alcoholic –OH, respectively, and the wide band at around 3400 cm^{-1} is further enhanced due to $–NH_2$ groups from CG, all these results highlight the successful conjugation of CG. At the same time, the disappearance of the fingerprint bands of HPW proves strong interaction between CG and the heteropolyacids, which is in good agreement with aforementioned XRD analysis results. However, the characteristic peaks of CG aforementioned considerably weaken in intensities and undergo position migrations after the immobilization of Ag NPs (Fig. 6(d)), it is easy to perceive that the amino groups and hydroxyl groups of CG have participated in the reduction and stability of Ag NPs, as expected.

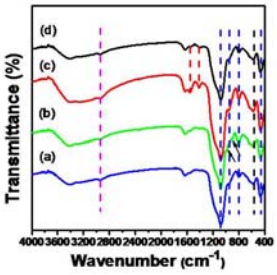

Fig. 6 FTIR spectra of Fe_3O_4@SN (a), Fe_3O_4@SN/HPW (b), Fe_3O_4@SN/ HPW@CG (c) and Fe_3O_4@SN/HPW@CG-Ag (d), respectively.

To further confirm the combination of CG and the formation of Ag NPs, the wide scan survey XPS of Fe_3O_4@SN/HPW@CG-Ag and the high resolution core level spectrum of the Ag element were carried out. According to the survey scan spectrum (Fig. 7A), we could only observe the signals of C, N, O, and Ag element indicating the successful modification of Fe_3O_4@SN/HPW by CG. Using the binding energy of C1s (284.6 eV) as a reference, the high resolution spectrum of Ag element was analyzed. It is clearly seen from Fig. 7B that the signals of Ag 3d are composed of doublet peaks at 367.8 and 373.8 eV corresponding to Ag $3d_{5/2}$ and Ag $3d_{3/2}$, respectively, which exhibit no obvious shift in comparison with those of bulk Ag (368.3 eV for Ag $3d_{5/2}$ and 374.3 eV for Ag $3d_{3/2}$).[49] Moreover, the gap between the two states is 6.0 eV. All the results demonstrate unambiguously that Ag in the composite is zero-valent and further testify that $AgNO_3$ has been reduced to Ag NPs by CG. The results are in accordance with the TEM, EDX, XRD and FTIR characterization results.

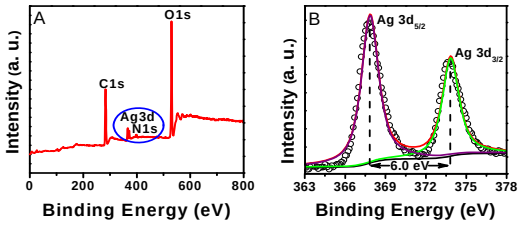

Fig. 7 (A) XPS survey spectra of Fe_3O_4@SN/HPW@CG-Ag catalysts and (B) high resolution core level spectra of Ag 3d .

The magnetic properties of Fe_3O_4@SN/HPW@CG-Ag catalysts were characterized through a vibrating sample magnetometer (VSM) at room temperature. Neither hysteresis loops nor remanence is detected in the magnetization curve (Fig. 8), suggesting that Fe_3O_4@SN/HPW@CG-Ag composites are superparamagnetic and the saturation magnetization value is measured to be 28.6 emu g^{-1}. Thus the as-prepared catalyst is capable of magnetic separation and recovery. As soon as the placement of a magnet beside the cuvette (Fig. 8, inset), Fe_3O_4@SN/HPW@CG-Ag in aqueous solution are attracted to the side of the cuvette leaving the solution transparent, which is the intuitive proof of their magnetic nature.

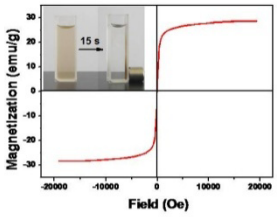

Fig. 8 Room temperature magnetization curve of Fe_3O_4@SN/HPW@CG-Ag catalysts .The inset photograph is the recovery process of Fe_3O_4@SN/HPW@CG-Ag aqueous solution by a magnet.

Catalytic test of Fe_3O_4@SN/HPW@CG-Ag NPs for 4-NP reduction. In order to assess the catalytic capability of Fe_3O_4@SN/HPW@CG-Ag nanocomposites, the reduction of 4-NP by $NaBH_4$ at room temperature was chosen as a model reaction, which is widely used as evaluation criteria of catalytic activity of metal nanoparticles.

The pure 4-NP solution exhibited a maximum absorption at 317 nm, no sooner than the addition of freshly prepared $NaBH_4$ solution, the absorption peak red shifted to 400 nm owing to the

formation of 4-nitrophenolate ion in alkaline condition (Fig. 9A). Meanwhile, the change occurring in the solution could also be observed visually (Fig. 9A, inset,), the light yellow color of 4-NP aqueous solution changed to bright yellow after adding $NaBH_4$ solution. It is noteworthy that, without suitable catalysts, the reduction of 4-NP with an excess amount of $NaBH_4$ could not occur even if it is thermodynamically favorable (E_0 for 4-NP/4-AP and H_3BO_3/BH_4^- are -0.76 and -1.33 V, respectively).

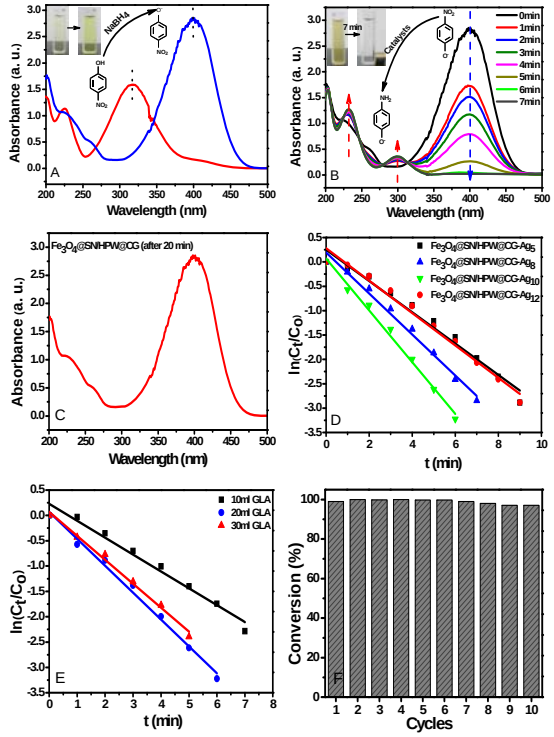

Fig. 9 (A) UV-vis absorption spectra of 4-NP with and without $NaBH_4$ solution. (B) Time-dependent UV-vis absorption spectra during the catalytic reduction of 4-NP by Fe_3O_4@SiO_2/HPW@CS-Ag at room temperature. (C) UV-vis absorption spectra of 4-NP with the addition of Fe_3O_4@SiO_2/HPW@CS after 20 min. The relationship between $\ln(C_t/C_0)$ and the reaction time for Fe_3O_4@SiO_2/HPW@CS-Ag with different $AgNO_3$ concentrations (D) and different GLA volumes (E). (F) The reusability of Fe_3O_4@SN/HPW@CG-Ag catalysts for the reduction of 4-NP by $NaBH_4$.

However, on introducing small amount of Fe_3O_4@SN/HPW@CG-Ag nanoparticles (1 mL, 1.0 mg mL^{-1}), the reaction was performed. As shown in Fig. 9B, time-dependent UV-vis spectra of this catalytic reaction system displayed explicitly that the intensity of the characteristic absorption peak at 400 nm markedly decreased over time and nearly disappeared within 7 min coupled with the appearance of new peaks at 298 nm and 231 nm, which are the characteristic peaks of 4-AP, revealing the reduction of 4-NP to 4-AP. At the same time, the reduction of 4-NP could also be visually witnessed the bright yellow reaction solution gradually became colorless within 7 min (Fig. 9B, inset). Besides, bare Fe_3O_4@SN/HPW@CG instead of Fe_3O_4@SN/HPW@CG-Ag as catalyst was also studied as a control experiment. From Fig. 9C, no obvious change in the intensity of the absorption at 400 nm could be detected even after 20 min, undoubtedly confirming that the reduction of 4-NP by $NaBH_4$ is solely catalyzed by Ag NPs stabilized on Fe_3O_4@SN/HPW@CG. These results indicated that Fe_3O_4@SN/HPW@CG-protected Ag NPs indeed could catalyze the reduction process and the catalytic property is extremely high. Simply put, Ag NPs in the reaction system play the role of electronic transfer station between BH_4^- ions and 4-nitrophenolate ions. It was worth mentioning here that the reaction started immediately after the addition of catalysts, that is to say, there was no induction time needed, which might greatly facilitate the practical applications.

Considering the concentration of $NaBH_4$ is higher than that of 4-NP, the reaction rate constant could be assumed to be independent of the concentration of $NaBH_4$, thus the rate constant for the reduction of 4-NP could be evaluated by the pseudo-first-order kinetics. The ratios of C_t (the concentration of 4-NP at time t) to C_0 (the initial concentration of 4-NP) were calculated from the standard curve of absorbance versus concentration of 4-NP at 400 nm. As shown in Fig. 9D and e, a good linear relationship between $\ln(C_t/C_0)$ and reaction time is displayed, which is well consistent with the first-order kinetics. The kinetic reaction rate constants k calculated from the slope of the straight line in Fig. 9D are 0.3211, 0.4205, 0.5309 and 0.3321 min^{-1} for Fe_3O_4@SN/HPW@CG-Ag_5, Fe_3O_4@SN/HPW@CG-Ag_8, Fe_3O_4@SN/HPW@CG-Ag and Fe_3O_4@SN/HPW@CG-Ag_{12}, respectively. These results clearly indicated that Fe_3O_4@SN/HPW@CG-Ag possessed much higher catalytic activity than others, which is in good agreement with the result of TEM. This should be mainly attributed to the relatively uniform size and high density effects of Ag NPs in the composites. In contrast with the other three, Fe_3O_4@SN/HPW@CG-Ag posses more and much smaller Ag NPs as discussed above (Fig. 3C), which would significantly expedite the accessibility of 4-NP to active sites, therefore enhanced the catalytic activity. In other words, the amount of $AgNO_3$ plays an important role in the formation of Ag NPs and subsequent catalytic performance.

On the other hand, to investigate the impact of GLA on Ag^+ adsorption capacity, we have made a comparison of their catalytic reaction rates for 4-NP. As shown in Fig. 9E, when the volume of GLA were 10, 20, 30 mL (the concentration of $AgNO_3$ was set to 10×10^{-3} M), the corresponding rate constants k were calculated to be 0.3332, 0.5309 and 0.4725 min^{-1}, respectively. This could be explained that, when the volume of GLA was increased from 10 to 20 mL, more amino and hydroxyl active groups were released to adsorb more Ag^+. However, as the volume further increased to 30 ml, the adsorption capacity decreased slightly because the higher mechanical strength of CG layer affect the diffusion of Ag^+ into Fe_3O_4@SN/HPW@CG, which were supported by the results from EDX (Table 1) datum that the mass fraction of Ag were 5.96, 7.92, 7.46 for 10, 20, 30 mL, respectively.

Given the ability of practical or industrial applications, the regeneration capacity of catalytic activity seems to be extremely important. Hence, the reusability of Fe_3O_4@SN/HPW@CG-Ag was investigated via the reduction of 4-NP in this article. After each run of catalysis, the catalysts were separated from the reaction mixture rapidly and conveniently with an external magnetic field, rinsed with deionized water, and then reused in the next cycle. As shown in Fig. 9F, the nanocatalysts were successfully recycled and reused ten times with a conversation of $\geq$ 97%, which certified that Fe_3O_4@SN/HPW@CG could serve as a robust support for the deposition of Ag NPs, expectedly leading to high-

performance nanocatalyst towards the reduction of 4-NP under aqueous reaction conditions.

Conclusions

In summary, the magnetic recyclability of Fe_3O_4, the protective effect of SiO_2, the adsorption, stability, and green reduction ability of chitosan as well as the catalytic activity of Ag NPs were successfully integrated into a whole with a sturdy construction through the introduction of polyanion phosphotungstic acid. During this process, Ag NPs were in-situ green synthesized in aqueous solution and stabilized by chitosan in the absence of any other reducing agent or organic solvent, which were environmentally benign. In addition, the size and amount of the Ag NPs embedded in the chitosan shell could be readily controlled through varying the concentration of $AgNO_3$ and the volume of glutaraldehyde. Besides, the thickness of chitosan shell could be easily controlled by varying the addition amount of phosphotungstic acid. And above all, the as-prepared Fe_3O_4@SN/HPW@CG-Ag NPs exhibited excellent catalytic performance (e.g. completed within 7 min) and reusability (reused at least 10 times without significant loss of activity) for the reduction of 4-nitrophenol in the presence of sodium borohydride. Furthermore, the design strategy based on Fe_3O_4@SN/HPW@CG-Ag may provide a novel platform for the preparation of other multifunctional organic-inorganic hybrid nanocatalyst systems with long-term stability.

Acknowledgements

Financial support from the Natural Science Foundation of Liaoning Province (No.201202014) is highly appreciated.

Notes and references

[a] Faculty of Light Industry and Chemical Engineering, Dalian Polytechnic University, Dalian 116034, China.

1 H. Wang, J. Shen, G. X. Cao, Z. Gai, K. L. Hong, P. R-Debata, P. Banerjeea and S. Q. Zhou, *J. Mater. Chem. B*, 2013, **1**, 6225.
2 Y. H. Deng, C. C. Wang, X. Z. Shen, W. L. Yang, L. Jin, H. Gao and S. K. Fu, *Chem. Eur. J.* , 2005, **11**, 6006.
3 Z. U. Rahman, Y. L. Dong, L. Su, Y. H. M, H. J. Zhang and X. G. Chen, *Chem. Eng. J.* , 2013, **222**, 382.
4 S. H. Joo, J. Y. Park, C. K. Tsung, Y. Yamada, P. D. Yang and G. A. Somorjai, *Nat. Mater.* , 2009, **8**, 126.
5 X. Q. Liu, Y. P. Guan, Z. Y. Ma and H. Z. Liu, *Langmuir*, 2004, **20**, 10278.
6 N. C. Feitoza, T. D. Gonçalves, J. J. Mesquita, J. S. Menegucci, M. K. M. S. Santos, J. A. Chaker, R. B. Cunha, A. M. M. Medeiros, J. C. Rubim and M. H. Sousa, *J. Hazard. Mater.* , 2014, **264**, 153.
7 X. D. Wang, H. Y. Liu, D. Chen, X. W. Meng, T. L. Liu, C. H. Fu, N. J. Hao, Y. Q. Zhang, X. L. Wu, J. Ren and F. Q. Tang, *ACS Appl. Mater. Interf.* , 2013, **5**, 4966.
8 F. Hoffmann, M. Cornelius, J. Morell and M. Fröba. *Angew. Chem. Int. Ed.* , 2006, **45(20)**, 3216.
9 A. Roucoux, J. Schulz and H. Patin, *Chem. Rev.* , 2002, **102**, 3757.
10 S. Jansat, M. Gómez, K. Philippot, G. Muller, E. Guiu, C. Claver, S. Castillón and B. Chaudret, *J. Am. Chem. Soc.* , 2004, **126**, 1592.
11 D. Astruc, F. Lu and J. R. Aranzaes, *Angew. Chem. Int. Ed.* , 2005, **44**, 7852.
12 S. Y. Wei, Z. P. Dong, Z. Y. Ma, J. Sun and J. T. Ma, *Catal. Commun.* , 2013, **30**, 40.
13 Y. J. Guo, Z. W. Liu, G. J. Wang, Y. H. Huang and F. F. Kang, *Appl. Surf. Sci.* , 2011, **258**, 1082.
14 T. J. Yao, T. Y. Cui, X. Fang, F. Cui and J. Wu, *Nanoscale*, 2013, **5**, 5896.
15 B. Wang, K. Chen, S. Jiang, F. Reincke, W. J. Tong, D. Y. Wang and C. Y. Gao, *Biomacromolecules*, 2006, **7**, 1203.
16 H. Z. Huang, X. R. Yang, *Biomacromolecules*, 2004, **5**, 2340.
17 Y. C. Chang and D. H. Chen, *J. Colloid Interface Sci.* , 2005, **283**, 446.
18 N. Sohrabi, N. Rasouli and M. Torkzadeh, *Chem. Eng. J.* , 2014, **240**, 426.
19 P. Li, Y. Yu, H. Liu, C. Y. Cao and W. G. Song, *Nanoscale*, 2014, **6**, 4420.
20 M. Zhu, C. Wang, D. Meng and G. Diao, *J. Mater. Chem. A*, 2013, **1**, 2118.
21 M. Zhu and G. Diao, *Nanoscale*, 2011, **3**, 2748.
22 P. Li, Y. Yu, H. Liu, C. Y. Cao and W. G. Song, *Nanoscale*, 2014, **6**, 442.
23 B. Liu, X. M. Wang, Y. W. Zhao, J. C. Wang and X. L. Yang, *J. Colloid Interface Sci.* , 2013, **395**, 91.
24 J. R. Chiou, B. H. Lai, K. C. Hsu and D. H. Chen, *J. Hazard. Mater.* , 2013, **248-249**, 394.
25 R. J. Liu, X. L. Yu, G. J. Zhang, S. J. Zhang, H. B. Cao, A. Dolbecq, P. Mialane, B. Keitad and L. J. Zhi, *J. Mater. Chem. A*, 2013, **1**, 11961.
26 Y. Y. Li, D. Y. Yuan, M. J. Dong, Z. H. Chai and G. Q. Fu, *Langmuir*, 2013, **29 (37)**, 11770.
27 A. Gangula, R. Podila, R. M, L. Karanam, C. Janardhana and A. M. Rao, *Langmuir*, 2011, **27**, 15268.
28 H.Z. Huang and X.R. Yang, *Biomacromolecules*, 2004, **5**, 2340.
29 B. Wang, K. Chen, S. Jiang, F. Reincke, W.J. Tong, D.Y. Wang and C. Y. Gao, *Biomacromolecules*, 2006, **7**, 1203.
30 Z. G. Chen, Z. Wang, X. Chen, H. X. Xu and J. B. Liu, *J. Nanopart Res.* , 2013, **15**, 1930.
31 T. Miyama and Y. Yonezawa, *Langmuir*, 2004, **20**, 5918.
32 M. J. Laudenslager, J. D. Schiffman and C. L. Schauer, *Biomacromolecules*, 2008, **9**, 2682.
33 M. J. Hortigüela, I. Aranaz, M. C. Gutiérrez, M. L. Ferrer and F. del Monte, *Biomacromolecules*, 2011, **12**, 179.
34 A. Regiel, S. Irusta, A. Kyzioł, M. Arruebo and J. Santamaria, *Nanotechnology*, 2013, **24**, DOI: 10.1088/0957-4484/24/1/015101
35 S. Boufi, M. R. Vilar, A. M. Ferraria and A. M. B. do Rego, *Colloids and Surfaces A: Physicochem. Eng. Aspects*, 2013, **439**, 151.
36 C. Shen, Y. J. Wang, J. H. Xu and G. S. Luo, *Chem. Eng. J.* , 2013, **229**, 217.
37 B. Bolto, T. Tran, M. Hoang and Z. Xie, *Prog. Polym. Sci.* , 2009, **34**, 969.
38 N. Prakash, P. N. Sudha and N. G. Renganathan, *Environ. Sci. Pollut. Res.* , 2012, **19**, 2930.
39 A. G. Destaye, C. K. Lin and C. K. Lee, *ACS Appl. Mater. Interf.* , 2013, **5**, 474.
40 G. Z. Kyzas, P. I. Siafaka, D. A. Lambropoulou, N. K. Lazaridis and D. N. Bikiaris, *Langmuir*, 2013, DOI: 10.1021/la402778x
41 J. M. Zhang, S. R. Zhai, S Li, Z. Y. Xiao, Y Song, Q. D. An and G. Tian, *Chem. Eng. J.* , 2013, **215-216**, 461-471

42 J. M. Zhang, S. R. Zhai, B. Zhai, Q. D. An and G. Tian, *J. Sol-Gel Sci. Technol.* , 2012, **64**, 347.
43 J. M. Zheng, Y. L. Dong, W. F. Wang, Y. H. Ma, J. Hu, X. J. Chen and X. G. Chen, *Nanoscale*, 2013, **5**, 4894.
44 T. Zeng, X L. Zhang, H. Y. Niu, Y. R. Ma, W. H. Li and Y. Q. Cai, *Appl. Catal. B: Environmental*, 2013, **134-135**, 26.
45 M. Y. Zhu, C. J. Wang, D. H. Meng and G. W. Diao, *J. Mater. Chem. A*, 2013, **1**, 2118.
46 K. S. Shin, J. Y. Choi, C. S. Park, H. J. Jang and K. Kim, *Catal. Lett.* , 2009, **133**, 1.
47 Q. Yuan, Y. Chi, N. Yu, Y. Zhao, W. F. Yan, X. T. Li and B. Dong, *Mater. Res. Bull.* , 2014, **49**, 279.
48 Y. G. Zhao, J.X. Li, L. P. Zhao, S. W. Zhang, Y. S. Huang, X. L. Wu and X. K. Wang, *Chem. Eng. J.* , 2014, **235**, 275.

